Optimization of Continuous Tube Motion and Step-and-Shoot Motion in Digital Breast Tomosynthesis Systems with Patient Motion

Raymond J. Acciavatti and Andrew D. A. Maidment
University of Pennsylvania, Department of Radiology, 3400 Spruce St., Philadelphia PA 19104
E-mail: racci@seas.upenn.edu and Andrew.Maidment@uphs.upenn.edu

ABSTRACT

In digital breast tomosynthesis (DBT), a reconstruction of the breast is generated from projections acquired over a limited range of x-ray tube angles. There are two principal schemes for acquiring projections, continuous tube motion and step-and-shoot motion. Although continuous tube motion has the benefit of reducing patient motion by lowering scan time, it has the drawback of introducing blurring artifacts due to focal spot motion. The purpose of this work is to determine the optimal scan time which minimizes this trade-off. To this end, the filtered backprojection reconstruction of a sinusoidal input is calculated. At various frequencies, the optimal scan time is determined by the value which maximizes the modulation of the reconstruction. Although prior authors have studied the dependency of the modulation on focal spot motion, this work is unique in also modeling patient motion. It is shown that because continuous tube motion and patient motion have competing influences on whether scan time should be long or short, the modulation is maximized by an intermediate scan time. This optimal scan time decreases with object velocity and increases with exposure time. To optimize step-and-shoot motion, we calculate the scan time for which the modulation attains the maximum value achievable in a comparable system with continuous tube motion. This scan time provides a threshold below which the benefits of step-and-shoot motion are justified. In conclusion, this work optimizes scan time in DBT systems with patient motion and either continuous tube motion or step-and-shoot motion by maximizing the modulation of the reconstruction.

Keywords: Digital breast tomosynthesis (DBT), continuous tube motion, step-and-shoot motion, patient motion, image reconstruction, filtered backprojection, modulation, optimization.

1. INTRODUCTION

Digital breast tomosynthesis (DBT) is a 3D imaging modality in which tomographic sections of the breast are generated from a limited range of x-ray projections. Preliminary studies indicate that DBT has increased sensitivity and specificity for early cancer detection relative to conventional 2D digital mammography.[1] There are two main schemes for acquiring projection images in DBT, step-and-shoot motion and continuous tube motion. Systems with continuous tube motion have the benefit of shorter scan time and thus less patient motion; the trade-off is increased blurring due to focal spot motion. Using a prototype DBT system (Hologic Inc., Bedford, MA), Ren *et al*. showed that blurring due to focal spot motion increases with height above the breast support. At a 4.0 cm height, the projected distance traveled by the focal spot during a single exposure is approximately half the detector element length.[2]

According to Zhao, focal spot motion degrades the modulation transfer function (MTF) of each projection by sinc($a_1 f_r$), where a_1 is the projected distance traveled by the focal spot and f_r is radial frequency perpendicular to the ray of incidence. Because focal spot motion has no effect on noise power spectra (NPS), the degradation in detective quantum efficiency (DQE) is more pronounced than the degradation in MTF due to the dependency of DQE on the square of the MTF. At the alias frequency of 5.9 line pairs per millimeter (lp/mm) in a prototype system, Zhao found that focal spot motion degrades MTF and DQE by 30% and 50%, respectively.[3]

In order to minimize the blurring due to focal spot motion in a system with continuous tube motion, Bissonnette *et al.* proposed lengthening the scan time. They demonstrated that a 39 s scan time effectively eliminated image quality degradation due to focal spot motion in a prototype Siemens Novation™ system.[4] Unfortunately, it is not practical to employ a long scan time as it permits greater patient motion.

Medical Imaging 2012: Physics of Medical Imaging, edited by Norbert J. Pelc, Robert M. Nishikawa, Bruce R. Whiting, Proc. of SPIE Vol. 8313, 831306 · © 2012 SPIE · CCC code: 1605-7422/12/$18 · doi: 10.1117/12.911016

Figure 1 illustrates the blurring due to patient motion in clinical images acquired with the Selenia Dimensions system (Hologic Inc., Bedford, MA) and reconstructed with a commercial prototype backprojection filtering algorithm (Briona^{TM}, Real Time Tomography, Villanova, PA). A small region of interest (ROI) with two microcalcifications at the height 22.0 mm above the breast support is shown. This depth was found to minimize the motion of the microcalcifications in the 15 individual backprojections, and thus is the height above the breast support at which the microcalcifications are in focus. By comparing the positions of the microcalcifications relative to a fixed marker (×) among all backprojections at the 22.0 mm depth, the net displacements of the microcalcifications in the mediolateral direction (top-to-bottom in the figure) and the chest wall-to-nipple direction (left-to-right in the figure) are approximately 140 μm and 280 μm, respectively, corresponding to one- and two-times the length of a detector element. With a 3.7 s scan time, the microcalcification velocities are thus 38 μm/s and 76 μm/s in these two respective directions. The microcalcifications appear blurry and artificially enlarged in the reconstruction as a result of patient motion.

Although image quality degradation due to continuous tube motion has been modeled by many authors, no one has incorporated patient motion into the analysis. Because these two types of motion have competing influences on whether scan time should be very long or very short, one would expect image quality to be optimized by an intermediate scan time. For this reason, the purpose of this work is to determine the optimal scan time by maximizing the modulation of the reconstruction at various frequencies. To optimize step-and-shoot motion in a similar fashion, we calculate the scan time for which the modulation matches the maximum value achievable in a comparable system with continuous tube motion. This scan time provides a threshold below which the benefits of step-and-shoot motion are justified.

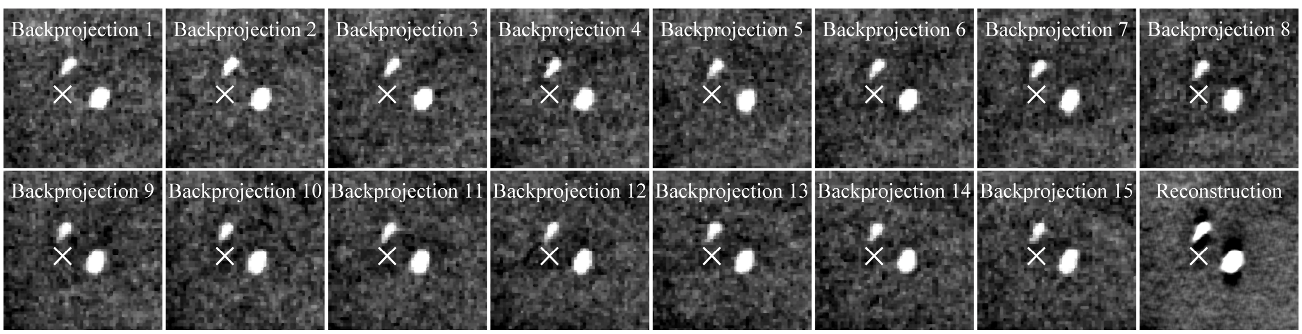

Figure 1. Backprojections of identical ROIs of clinical tomosynthesis images at a 22.0 mm height above the breast support are shown. This height was found to minimize the motion of the microcalcifications, ensuring that the microcalcifications are in focus in the corresponding reconstructed slice. The microcalcifications shift position relative to a fixed marker (×) in the 15 individual backprojections. Such patient motion causes blurring and artificial enlargement of the microcalcifications in the reconstruction.

2. METHODS

2.1 Acquisition Geometry for Continuous Tube Motion (CTM)

In order to calculate the scan time which optimizes the modulation of a DBT reconstruction at various frequencies, it is first necessary to model the acquisition geometry. We simulate a DBT system in which the detector rotates in synchrony with the x-ray tube during the acquisition of the projections. As diagrammed schematically in Figure 2, the x-ray tube rotates within the plane of the chest wall (*i.e.*, the xz plane) about the origin O, corresponding to the midpoint of the chest wall side of the detector. In addition, the detector rotates about the y axis, with O acting as the pivot point. At the x-ray tube angle ψ relative to the z axis, the detector rotation angle (γ) is found from the ratio ψ/g, where g is the gear ratio of the detector. Positive directionalities of ψ and γ are defined as those presented in Figure 2, and in the limit $g \to \infty$, a stationary detector can be recovered ($\gamma \to 0$).

In a system with continuous tube motion at a constant angular velocity ω, each projection is acquired over the exposure time τ as the tube is swept over the angular extent $\Psi = \omega\tau$. For the n^{th} projection, the x-ray tube arc is centered about the angle $\psi_n = n\Delta\psi$, so that the x-ray tube angle varies between $\psi = \psi_n + \Psi/2$ and $\psi = \psi_n - \Psi/2$ during the exposure time τ. In the literature, ψ_n is often termed the nominal projection angle and $\Delta\psi$ the angular spacing between projections.[5] With an odd number of N total projections, the index n varies between $-(N-1)/2$ and $(N-1)/2$, and the special case $n = 0$ defines the central projection. Denoting the total scan time as T_t, the total angular range of the x-ray tube motion can be

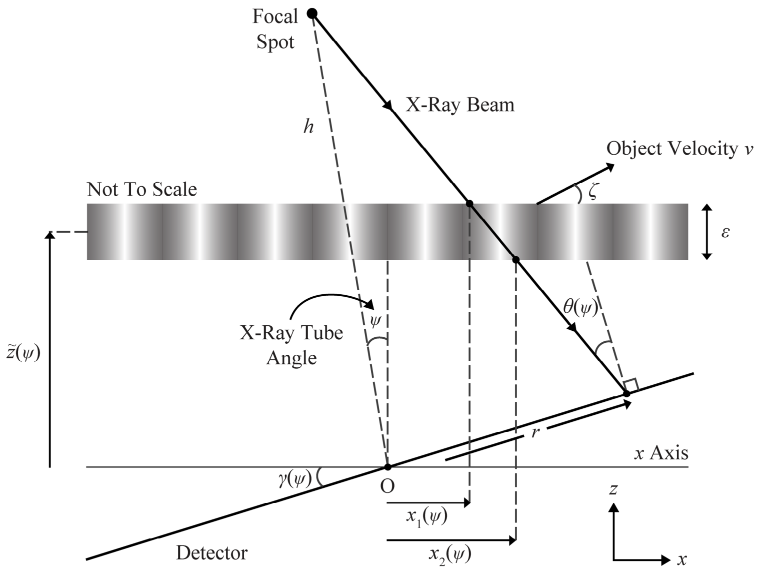

Figure 2. A diagram of the acquisition geometry is shown (not to scale). The attenuation coefficient of the input object varies sinusoidally along the x direction. To model patient motion, the input object has velocity v at the angle ζ relative to the x direction.

written as ωT_t, or equivalently, as the difference between the initial x-ray tube angle (ψ_i) and the final x-ray tube angle (ψ_f).

$$\omega T_t = \psi_i - \psi_f = \left(\frac{N-1}{2}\right)\Delta\psi + \frac{\Psi}{2} - \left[-\left(\frac{N-1}{2}\right)\Delta\psi - \frac{\Psi}{2}\right] = (N-1)\Delta\psi + \Psi \tag{1}$$

Substituting $\omega = \Psi/\tau$ in the left-hand side of Eq. (1), the angular sweep of the x-ray tube over the exposure time τ can be expressed in terms of the total scan time T_t instead of the tube's angular velocity ω.

$$\Psi = \left(\frac{N-1}{T_t - \tau}\right)\tau\Delta\psi \tag{2}$$

This formula for Ψ is useful as the total scan time is more directly measurable than the tube's angular velocity.

2.2 Detector Signal for Sinusoidal Input to CTM System

A framework for investigating tube motion and patient motion in DBT is now developed by calculating the modulation of the reconstruction of a sinusoidal input. Accordingly, suppose that a thin rectangular plate with its long axis parallel to the breast support possesses a linear attenuation coefficient $\mu(x, z)$ which varies sinusoidally with position x. Although an actual input to a clinical breast imaging system would be 3D, a 2D construct is a useful tool for simulating measurements in the plane of the chest wall. The extension of this framework to measurements made perpendicular to the chest wall is reserved for future work.

As shown in Figure 2, the rectangular plate is positioned between $z = \tilde{z}(\psi) - \varepsilon/2$ and $z = \tilde{z}(\psi) + \varepsilon/2$, where $\tilde{z}(\psi)$ is the central height of the plate above the detector at the x-ray tube angle ψ and ε is the plate's thickness. The height $\tilde{z}(\psi)$ is taken to be dependent upon the x-ray tube angle ψ in order to model the presence of patient motion. For an input frequency f_0, the attenuation coefficient may be written

$$\mu(x,z) = C \cdot \cos\left(2\pi f_0 \left[x - \tilde{x}(\psi)\right]\right) \cdot \mathrm{rect}\left[\frac{z - \tilde{z}(\psi)}{\varepsilon}\right], \qquad \mathrm{rect}(u) \equiv \begin{cases} 1 & ,|u| \le 1/2 \\ 0 & ,|u| > 1/2 \end{cases}, \tag{3}$$

where C is the amplitude of the sinusoidal waveform and $\tilde{x}(\psi)$ is its translational shift along the x direction. Provided that $|z - z_0| \leq \varepsilon$, the Fourier transform of Eq. (3) along the x direction is a linear sum of delta functions[5] which peak at the frequencies $f = \pm f_0$. Typically, only the positive frequency $f = +f_0$ is of interest in an experimental measurement. Hence, although it is non-physical for a linear attenuation coefficient to vary between negative and positive values, formulating $\mu(x, z)$ by Eq. (3) is helpful for a thought experiment in the reconstruction of a single input frequency.

In Figure 2, the displacements $x_1(\psi)$ and $x_2(\psi)$ determine the entrance and exit points of the x-ray beam through the sine plate for the incident point on the detector at a distance r from O. Following our previous work,[5] $x_1(\psi)$ and $x_2(\psi)$ can be written as $x_1(\psi) = \rho(\psi)\cdot r - \lambda^+(\psi)$ and $x_2(\psi) = \rho(\psi)\cdot r - \lambda^-(\psi)$, where $\rho(\psi) \equiv \cos[\gamma(\psi)] + \sin[\gamma(\psi)]\tan[\theta(\psi) + \gamma(\psi)]$ and $\lambda^{\pm}(\psi) \equiv [\tilde{z}(\psi) \pm \varepsilon/2]\cdot\tan\left[\theta(\psi)+\gamma(\psi)\right]$. The expression for the incident angle relative to the normal to the detector also follows from our previous work

$$\theta(\psi) = -\gamma(\psi) + \arctan\left(\frac{h\sin\psi + r\cos\left[\gamma(\psi)\right]}{h\cos\psi - r\sin\left[\gamma(\psi)\right]}\right), \tag{4}$$

where h is the source-to-origin distance (Figure 2). Total attenuation $\mathcal{A}\mu(\psi)$ recorded by the x-ray converter at the tube angle ψ may now be calculated by integrating the attenuation coefficient of the sine plate over the path length $\mathcal{L}(\psi)$.

$$\mathcal{A}\mu(\psi) = \int_{\mathcal{L}(\psi)} \mu ds = \int_{x_1(\psi)}^{x_2(\psi)} C\cdot\cos\left(2\pi f_0\left[x - \tilde{x}(\psi)\right]\right)\cdot\csc\left[\theta(\psi)+\gamma(\psi)\right]dx \tag{5}$$

In order to calculate the total attenuation $\mathcal{A}\mu(n)$ recorded by the x-ray converter for the n^{th} projection, one must integrate $\mathcal{A}\mu(\psi)$ over the angular arc swept by the x-ray tube during the exposure time τ.

$$\mathcal{A}\mu(n) = \int_{\psi_n-\Psi/2}^{\psi_n+\Psi/2}\int_{x_1(\psi)}^{x_2(\psi)} C\cdot\cos\left(2\pi f_0\left[x-\tilde{x}(\psi)\right]\right)\cdot\csc\left[\theta(\psi)+\gamma(\psi)\right]dx\frac{d\psi}{\Psi} \tag{6}$$

$$= \frac{C}{2\pi f_0}\int_{\psi_n-\Psi/2}^{\psi_n+\Psi/2}\csc\left[\theta(\psi)+\gamma(\psi)\right]\cdot\left[\begin{array}{l}\sin\left(2\pi f_0\left[\rho(\psi)\cdot r - \lambda^-(\psi) - \tilde{x}(\psi)\right]\right)\\ -\sin\left(2\pi f_0\left[\rho(\psi)\cdot r - \lambda^+(\psi) - \tilde{x}(\psi)\right]\right)\end{array}\right]\frac{d\psi}{\Psi} \tag{7}$$

Eq. (7) provides an expression for signal intensity versus position r along the detector, assuming that the detector is non-pixilated and possesses a modulation transfer function (MTF) of unity at all frequencies. An amorphous selenium (a-Se) photoconductor operated in drift mode is a good approximation for a detector with these properties.[6]

Total attenuation for the n^{th} projection can now be simplified using a sum-to-product trigonometric identity for real numbers α and β; namely, $\sin\alpha - \sin\beta = 2\cos[(\alpha+\beta)/2]\sin[(\alpha-\beta)/2]$

$$\begin{aligned}\mathcal{A}\mu(n) = C\varepsilon\int_{\psi_n-\Psi/2}^{\psi_n+\Psi/2} &\sec\left[\theta(\psi)+\gamma(\psi)\right]\operatorname{sinc}\left[\varepsilon f_0\tan\left[\theta(\psi)+\gamma(\psi)\right]\right]\\ &\cdot\cos\left[2\pi f_0\left[\rho(\psi)\cdot r - \tilde{z}(\psi)\cdot\tan\left[\theta(\psi)+\gamma(\psi)\right] - \tilde{x}(\psi)\right]\right]\frac{d\psi}{\Psi}\end{aligned}, \qquad \operatorname{sinc}(u) \equiv \frac{\sin(\pi u)}{\pi u}. \tag{8}$$

Because it is difficult to perform the integration in Eq. (8) in closed form, it is necessary to use approximation techniques. One such method is the midpoint formula. For the n^{th} projection, the angular sweep of the x-ray tube can be divided into K intervals between $\psi = \psi_n + \Psi/2$ and $\psi = \psi_n - \Psi/2$. The tube angle at the midpoint of the k^{th} interval is

$$\psi_{kn} = \psi_n - \frac{\Psi}{2}\left(1 - \frac{2k-1}{K}\right) = \left[n - \frac{\tau}{2}\left(\frac{N-1}{T_t - \tau}\right)\left(1 - \frac{2k-1}{K}\right)\right]\Delta\psi, \quad k \in \mathbb{N}. \tag{9}$$

Eq. (8) can now be evaluated by averaging the integrand over each of the K intervals in the limit of infinite K

$$\mathcal{A}\mu(n)=\lim_{K\to\infty}\frac{C\varepsilon}{K}\sum_{k=1}^{K}\sec(\theta_{kn}+\gamma_{kn})\mathrm{sinc}\left[\varepsilon f_0\tan(\theta_{kn}+\gamma_{kn})\right]\cos\left[2\pi f_0\left[\rho_{kn}r-\tilde{z}_{kn}\tan(\theta_{kn}+\gamma_{kn})-\tilde{x}_{kn}\right]\right], \tag{10}$$

where θ_{kn}, γ_{kn}, and ρ_{kn} are calculated by evaluating $\theta(\psi)$, $\gamma(\psi)$, and $\rho(\psi)$ at $\psi = \psi_{kn}$. In Eq. (10), the displacements $\tilde{x}_{kn}$ and $\tilde{z}_{kn}$ determine the position of the sine plate at the time point T_{kn}. The special case $T_{kn} = 0$ is defined to occur at the x-ray tube angle $\psi = 0$, so that the scan time occurs between the time points $-T_t/2$ and $T_t/2$.

$$T_{kn}=\frac{\psi_{kn}}{\omega}=\frac{\tau\psi_{kn}}{\Psi}=\left(\frac{T_t-\tau}{N-1}\right)\frac{\psi_{kn}}{\Delta\psi},\qquad \frac{-T_t}{2}\le T_{kn}\le\frac{T_t}{2} \tag{11}$$

To model the presence of patient motion, the sine plate is taken to have constant velocity v at the angle ζ relative to the x direction (Figure 2). The displacements $\tilde{x}_{kn}$ and $\tilde{z}_{kn}$ can be written in terms of the velocity components v_x and v_z as

$$\tilde{x}_{kn}=x_0+T_{kn}v_x=x_0+\left(\frac{T_t-\tau}{N-1}\right)\frac{v\psi_{kn}\cos\zeta}{\Delta\psi},\qquad \tilde{z}_{kn}=z_0+T_{kn}v_z=z_0+\left(\frac{T_t-\tau}{N-1}\right)\frac{v\psi_{kn}\sin\zeta}{\Delta\psi}, \tag{12}$$

where x_0 and z_0 are positions which determine the location of the sine plate at the x-ray tube angle $\psi = 0$.

In a digital detector, the *a*-Se x-ray converter is placed in electrical contact with a large area plate of amorphous silicon (*a*-Si) in which a thin-film transistor (TFT) array samples the total attenuation in pixels (*i.e.*, detector elements). Using Eq. (10), the logarithmically-transformed signal in the m^{th} detector element for the n^{th} projection is

$$\mathcal{D}\mu(m,n)=\int_{a(m-1/2)}^{a(m+1/2)}\mathcal{A}\mu(n)\cdot\frac{dr}{a}. \tag{13}$$

Detector elements are taken to be centered on $r = ma$, and the detector element containing O is the one corresponding to $m = 0$. Because the incident angle varies minimally within each detector element, the integration in Eq. (13) can be evaluated by approximating the incident angle θ_{kn} with its value at the centroid of the detector element. Thus

$$\mathcal{D}\mu(m,n)=\lim_{K\to\infty}\sum_{k=1}^{K}\frac{C\varepsilon\sec(\theta_{kmn}+\gamma_{kn})\cdot\mathrm{sinc}\left[\varepsilon f_0\tan(\theta_{kmn}+\gamma_{kn})\right]}{2\pi a\rho_{kmn}f_0K}\begin{bmatrix}\sin\left[2\pi f_0\left(a\rho_{kmn}(m+1/2)-\tilde{z}_{kn}\tan(\theta_{kmn}+\gamma_{kn})-\tilde{x}_{kn}\right)\right]\\-\sin\left[2\pi f_0\left(a\rho_{kmn}(m-1/2)-\tilde{z}_{kn}\tan(\theta_{kmn}+\gamma_{kn})-\tilde{x}_{kn}\right)\right]\end{bmatrix} \tag{14}$$

where θ_{kmn} and ρ_{kmn} are calculated by evaluating θ_{kn} and ρ_{kn} at $r = ma$. Eq. (14) can be simplified further by using the sum-to-product trigonometric identity described previously.

$$\begin{aligned}\mathcal{D}\mu(m,n)=\lim_{K\to\infty}\frac{C\varepsilon}{K}\sum_{k=1}^{K}&\sec(\theta_{kmn}+\gamma_{kn})\cdot\mathrm{sinc}\left[\varepsilon f_0\tan(\theta_{kmn}+\gamma_{kn})\right]\cdot\mathrm{sinc}\left[a\rho_{kmn}f_0\right]\\&\cdot\cos\left[2\pi f_0\left[ma\rho_{kmn}-\tilde{z}_{kn}\tan(\theta_{kmn}+\gamma_{kn})-\tilde{x}_{kn}\right]\right]\end{aligned} \tag{15}$$

2.3 Detector Signal for Step-and-Shoot Motion (SSM)

In a similar fashion, detector signal for a system with step-and-shoot motion can be calculated. All expressions between Eqs. (4) and (8) continue to hold, so that the total attenuation recorded by the x-ray converter for the n^{th} projection is

$$\mathcal{A}\mu(n)=C\varepsilon\sec(\theta_n+\gamma_n)\mathrm{sinc}\left[\varepsilon f_0\tan(\theta_n+\gamma_n)\right]\int_{T_n-\tau/2}^{T_n+\tau/2}\cos\left[2\pi f_0\left[\rho_n r-\tilde{z}(T)\cdot\tan(\theta_n+\gamma_n)-\tilde{x}(T)\right]\right]\frac{dT}{\tau}. \tag{16}$$

Because the x-ray tube angle ψ remains constant during a single projection in a system with step-and-shoot motion, it is acceptable to simplify Eq. (8) by evaluating $\theta(\psi)$, $\gamma(\psi)$, and $\rho(\psi)$ at the nominal projection angle $\psi = \psi_n$ as denoted by the parameters θ_n, γ_n, and ρ_n, respectively. Although the object coordinates $\tilde{x}(\psi)$ and $\tilde{z}(\psi)$ are dependent upon the x-ray tube angle ψ in a system with continuous tube motion, the same coordinates are now dependent upon time T. Consequently, the integral over ψ in Eq. (8) can be replaced by an integral over T to take into account the presence of patient motion. The integration limits in Eq. (16) are thus the initial and final time points at which the tube emits x rays during a single projection, where T_n is the central time point of the projection of duration τ and ΔT is the time difference between consecutive projections. It can be shown that $T_n = n(\tau + \Delta T)$ and $\Delta T = (T_t - N\tau)/(N-1)$. Substituting the object coordinates $\tilde{x}(T) = x_0 + vT\cos\zeta$ and $\tilde{z}(T) = z_0 + vT\sin\zeta$ into Eq. (16) yields

$$\begin{aligned}\mathcal{A}\mu(n) = C\varepsilon\sec(\theta_n+\gamma_n)\operatorname{sinc}\left[\varepsilon f_0\tan(\theta_n+\gamma_n)\right]\operatorname{sinc}\left[f_0\tau v\left[\cos\zeta+\sin(\zeta)\tan(\theta_n+\gamma_n)\right]\right] \\ \cdot\cos\left[2\pi f_0\left[\rho_n r-(x_0+vT_n\cos\zeta)-(z_0+vT_n\sin\zeta)\tan(\theta_n+\gamma_n)\right]\right]\end{aligned}. \tag{17}$$

By integrating $\mathcal{A}\mu(n)$ over the detector element length a [Eq. (13)], the logarithmically-transformed signal in the m^{th} detector element for the n^{th} projection can be determined

$$\begin{aligned}\mathcal{D}\mu(m,n) = C\varepsilon\sec(\theta_{mn}+\gamma_n)\operatorname{sinc}\left[\varepsilon f_0\tan(\theta_{mn}+\gamma_n)\right]\operatorname{sinc}\left[f_0\tau v\left[\cos\zeta+\sin(\zeta)\tan(\theta_{mn}+\gamma_n)\right]\right]\operatorname{sinc}\left[f_0 a\rho_{mn}\right] \\ \cdot\cos\left[2\pi f_0\left[ma\rho_{mn}-(x_0+vT_n\cos\zeta)-(z_0+vT_n\sin\zeta)\tan(\theta_{mn}+\gamma_n)\right]\right]\end{aligned}, \tag{18}$$

where θ_{mn} and ρ_{mn} are calculated by evaluating θ_n and ρ_n at $r = ma$.

2.4 Filtered Backprojection (FBP) Reconstruction

The attenuation coefficient can now be reconstructed using filtered backprojection (FBP). From our previous work,[5] the FBP reconstruction for an infinitesimally fine (*i.e.*, non-pixilated) reconstruction grid is given by the expression

$$\mu_{\text{FBP}}(x,z) = \frac{1}{N}\sum_m\sum_n \mathcal{D}\mu(m,n)\cdot\left[\phi(t)*\operatorname{rect}\left(\frac{t\sec\theta_{mn}-ma}{a}\right)\right]\Bigg|_{t=x\cos(\gamma_n+\theta_{mn})+z\sin(\gamma_n+\theta_{mn})}, \tag{19}$$

where μ_{FBP} is the reconstructed attenuation coefficient and $*$ is the convolution operator. The reconstruction filter $\phi(t)$ follows from linear systems theory for DBT. A ramp (RA) filter, given by $|f|$ in the Fourier domain, is first applied to reduce the low frequency detector response. Since noise tends to occur at high frequencies, a spectrum apodization (SA) filter is also used; following Zhao's approach,[3] we apply a Hanning window function as the SA filter. In the Fourier domain, the filters are truncated at the frequencies $f = \pm\xi$, and the net filter is the product of the RA and SA filters. As shown in our previous work,[5] the net filter can be calculated in closed form using the inverse Fourier transform.

3. RESULTS

Reconstructions are now simulated for a Selenia Dimensions system with 15 projections acquired at an angular spacing ($\Delta\psi$) of 1.07°, assuming $C = 1.0$ mm^{-1}, $h = 70.0$ cm, $\varepsilon = 0.50$ mm, and $a = 140$ µm. At the x-ray tube angle $\psi = 0$, the centroid of the sine plate is taken to coincide with the midpoint of the chest wall side of a 50.0 mm thick breast. With the breast support positioned 25.0 mm above the origin of the detector, the x_0 and z_0 coordinates of the input object are therefore 0 and 50.0 mm, respectively.

3.1 Effect of Continuous Tube Motion on Modulation

The effect of continuous tube motion on modulation is analyzed in Figure 3(a) by first simulating a system with no patient motion. For a 30.0 ms exposure time, corresponding to the mean value of τ for the Selenia Dimensions system, reconstructions of the frequency 2.0 lp/mm are calculated. As expected, the modulation increases with scan time. For example, with scan times of 2.0, 3.0, and 4.0 s, the modulation attains the values 0.59, 0.70, and 0.74, respectively. This trend arises because the tube's angular sweep Ψ during a single projection decreases with scan time [Eq. (2)].

For the same DBT system, the modulation in the reconstruction is also studied as a function of the input frequency f_0 [Figure 3(c)]. At low frequencies, the modulation increases linearly from zero, following the ramp filter. At higher frequencies, the spectrum apodization filter and the MTF of the detector sampling process reduce the modulation, countering the ramp filter; hence, there is an intermediate frequency at which the modulation is maximized. This frequency dependence of the modulation matches Zhao's formulation of in-plane MTF in DBT reconstructions,[3] providing a built-in check on the validity of Figure 3(c). Like Zhao, we plot the modulation over a frequency range

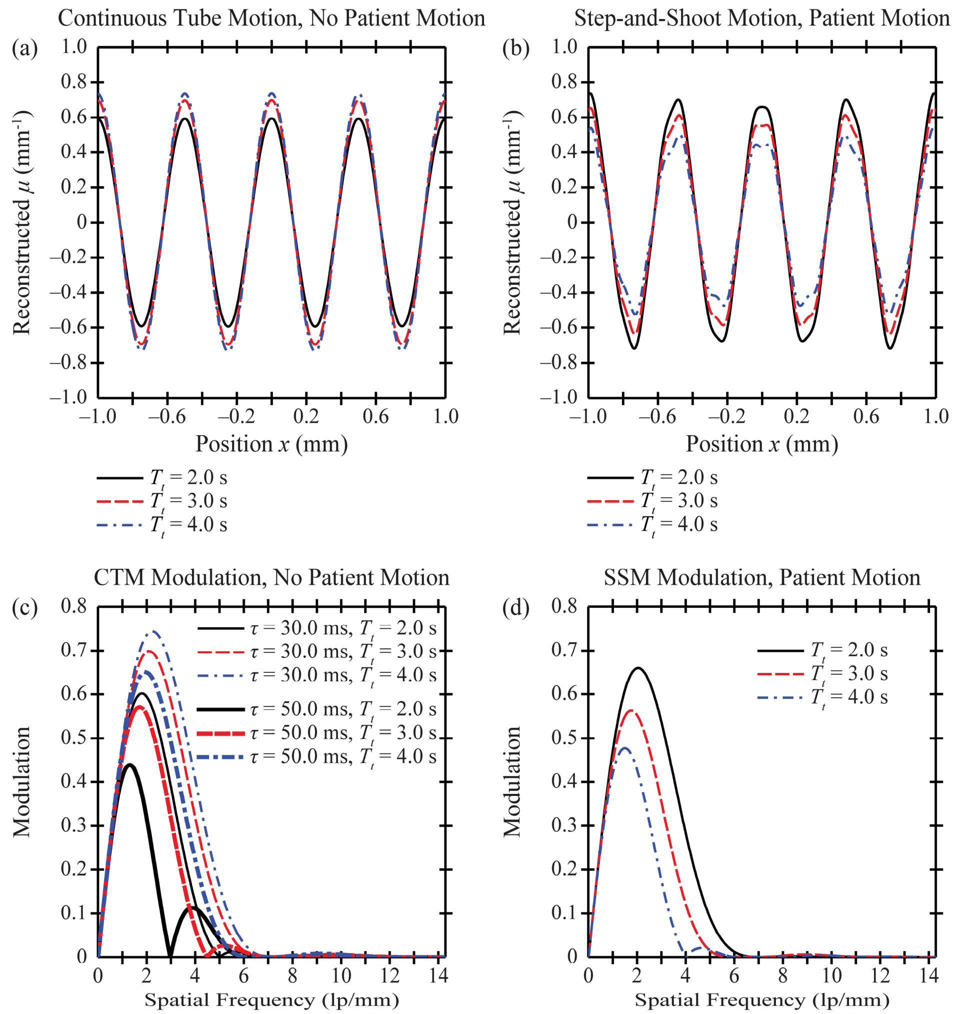

Figure 3. Although modulation increases with scan time in a system with continuous tube motion and no patient motion, the opposite trend holds in a system with step-and-shoot motion and patient motion.

spanning at least one zero of the MTF of the sampling process in the detector.[7] The filter truncation frequency (ξ) of $2a^{-1}$ (14.3 lp/mm) is simulated, corresponding to the second zero of the detector sampling MTF [sinc(af)]. Figure 3(c) shows that increasing the scan time increases the modulation of the reconstruction, and thus generalizes the trend presented in Figure 3(a) to all frequencies. By contrast, increasing the exposure time decreases the modulation.

In addition, Figure 3(c) demonstrates that the modulation of the reconstruction may possess zeros at frequencies different from those of the detector sampling MTF, whose first and second zero are a^{-1} (7.1 lp/mm) and $2a^{-1}$ (14.3 lp/mm). Increasing the exposure time decreases these additional zeros, while increasing the scan time increases the zeros. For a 50.0 ms exposure time, the first zero not equivalent to a^{-1} or $2a^{-1}$ is 3.0, 4.5, and 6.0 lp/mm for 2.0, 3.0, and 4.0 s scan times (5.0, 7.6, and 10.1 lp/mm for a 30.0 ms exposure time). The appendix shows that the formula for these zeros follows from the calculation of the MTF of focal spot motion. These zeros place an important limit on the resolution of the system.

3.2 Effect of Patient Motion on Modulation

In Figure 3(b), the effect of patient motion on modulation is investigated by considering a system with step-and-shoot motion. With an exposure time of 30.0 ms and an object velocity of 60.0 μm/s oriented along the x direction, Figure 3(b) demonstrates that modulation decreases with scan time. The object velocity considered in Figure 3(b) is comparable to the value observed in Figure 1 showing clinical images of microcalcifications. The modulation attains the values 0.66,

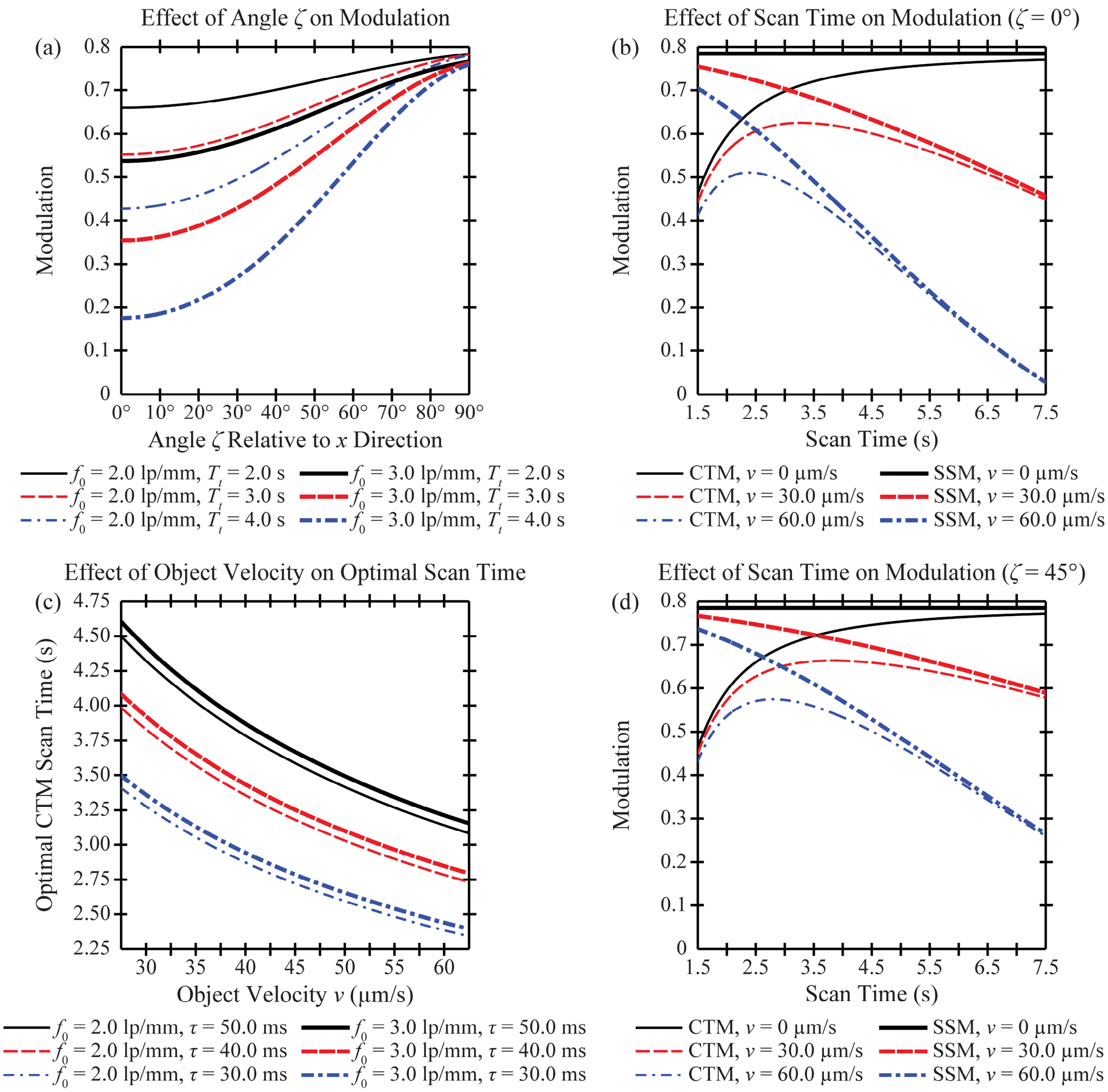

Figure 4. (a) By increasing the angle ζ of patient motion relative to the x direction, the modulation of the reconstruction increases. (b) With continuous tube motion (CTM) and patient motion occurring simultaneously, modulation is optimized by an intermediate scan time. By contrast, modulation is maximized by a short scan time with step-and-shoot motion (SSM). (c) The dependency of the optimal CTM scan time on object velocity (v), exposure time (τ), and frequency (f_0) is investigated. (d) The optimal CTM scan time is larger with patient motion oriented at a 45° angle relative to the x direction than a 0° angle [Figure 4(b)].

0.55, and 0.43 for 2.0, 3.0, and 4.0 s scan times, respectively. This dependency of modulation on scan time is expected since the net displacement of the object in the x direction, given by $vT_t\cos\zeta$, increases with scan time.

In Figure 3(d), modulation is plotted versus f_0 for a 30.0 ms exposure time. Figure 3(d) shows that the modulation decreases with scan time over all frequencies, thus generalizing the trend shown in Figure 3(c). Unlike a system with continuous tube motion and no patient motion, modulation varies minimally with exposure time in a system with step-and-shoot motion and patient motion. This finding arises because the object displacement between projections is significantly greater than the corresponding motion during the exposure time of an individual projection.

It is also demonstrated in Figure 3(d) that the frequency corresponding to the first zero of the modulation may be less than that of the detector sampling MTF. This zero follows from the point spread function (PSF) of patient motion, which is a rectangle function whose width is the object displacement during the scan time. Accordingly, the MTF of patient motion is sinc($vT_t f\cos\zeta$), and the first zero is $(vT_t)^{-1}\sec\zeta$. With scan times of 2.0, 3.0, and 4.0 s, the zeros of the MTF of patient motion are 8.3, 5.6, and 4.2 lp/mm, respectively, effectively matching the values in Figure 3(d).

In the same system, Figure 4(a) studies the dependence of modulation on the directionality of patient motion. At any fixed frequency, the modulation increases with the angle ζ relative to the x direction. In addition, the difference in modulation comparing any two scan times is minimized as ζ increases. Modulation is virtually independent of scan time if the patient motion is oriented along the z direction ($\zeta = 90°$).

3.3 Optimization of Scan Time

With both continuous tube motion and patient motion occurring simultaneously, there is a trade-off in the benefits of long and short scan time, and hence modulation is maximized by an intermediate scan time [Figure 4(b)]. For example, with object velocities (v) of 30.0 and 60.0 μm/s oriented along the x direction, the optimal scan times for continuous tube motion are 3.3 and 2.4 s, respectively, assuming an input frequency of 2.0 lp/mm and an exposure time of 30.0 ms. Figure 4(c) demonstrates that this optimal scan time decreases with object velocity (v) and increases with exposure time (τ). Exposure times between 30.0 ms (the mean value of the Selenia Dimensions system) and 50.0 ms (the maximum value of the system) are considered. Figure 4(c) also shows that the optimal scan time is frequency dependent.

For any fixed scan time, step-and-shoot motion (SSM) yields greater modulation than continuous tube motion (CTM). To optimize a step-and-shoot system, one may calculate the scan time giving the same modulation as the highest achievable with continuous tube motion [Figure 4(b)]. This scan time provides a threshold below which the use of step-and-shoot motion is justified. For example, with 30.0 μm/s patient motion, an SSM scan time of 4.7 s yields the same modulation as the optimal CTM scan time of 3.3 s. With 60.0 μm/s patient motion, the analogous SSM and CTM scan times are 3.3 and 2.4 s.

The dependence of the optimal CTM scan time on the directionality of patient motion is investigated in Figure 4(d) by considering patient motion along a 45° angle relative to the x direction. The optimal scan time for continuous tube motion is larger in Figure 4(d) than in Figure 4(b) with $\zeta = 0°$. For example, with an object velocity (v) of 30.0 μm/s, the optimal CTM scan times for $\zeta = 0°$ and 45° are 3.3 and 3.8 s, respectively (2.4 and 2.8 s for $v = 60.0$ μm/s). In addition, with $\zeta = 45°$, there is a broader range of scan times for which the modulation is within the limit of resolution of the system, which is often taken to be 0.05. For example, with an object velocity of 60.0 μm/s and a scan time of 7.5 s, the modulation with $\zeta = 45°$ is 0.26 (resolvable), yet the modulation with $\zeta = 0°$ is 0.03 (not resolvable).

4. DISCUSSION AND CONCLUSION

To our knowledge, this work is the first to model both continuous tube motion and patient motion in DBT, and as a result, to develop a technique which optimizes scan time. Continuous tube motion and patient motion have competing influences on scan time; we show that the modulation of the reconstruction is optimized by an intermediate scan time.

In Figure 4, it is demonstrated that continuous tube motion and step-and-shoot motion have nearly identical modulation in systems with very long scan time. For example, with a 2.0 lp/mm input and a 30.0 ms exposure time, one can show that the relative difference in modulation between the two systems does not exceed 1.0% for scan times of 10 s or more. This result holds regardless of the object velocity studied in Figure 4. For this reason, there is effectively no difference in image quality between the two systems if both operate at the same, very long scan time; patient motion is a much more significant cause of image quality degradation than continuous tube motion at these scan times.

To minimize patient motion in DBT, the system should have a short scan time comparable to 2D digital mammography. In systems with continuous tube motion, the drawback of lowering the scan time is substantial reduction of the modulation relative to an analogous step-and-shoot system (Figure 4). Since systems with step-and-shoot motion tend to have longer scan times than those with continuous tube motion due to mechanical considerations, Figure 4 demonstrates that it is still possible to operate a system with continuous tube motion at a scan time yielding superior image quality relative to a step-and-shoot system. An additional benefit of continuous tube motion might include eliminating microphonic vibrations during the exposure time of each projection.

In conventional 2D digital mammography, it has been demonstrated that the scan time should be less than 2.0 s to minimize patient motion. Currently, no such guideline for DBT has been developed. In order to optimize scan time in systems with continuous tube motion, our simulations considered object velocities between 30.0 and 60.0 μm/s. These velocities were chosen to be comparable to values seen in clinical images of microcalcifications presented in Figure 1. Although Figure 1 illustrates motion of microcalcifications in one clinical data set, the case is not necessarily representative of the most significant extent of patient motion, and thus additional cases should be considered in developing guidelines for scan time in DBT.

In systems with continuous tube motion, this paper demonstrates that the modulation of the reconstruction may be zero at frequencies smaller than the zeros of the MTF of detector sampling. This finding has important implications on the visibility of high frequencies in DBT, which was the subject of our prior work.[5] In performing reconstructions on a grid whose pixel size is much smaller than the detector elements, we have previously demonstrated that DBT is capable of super-resolution. Although the alias frequency of the Selenia Dimensions detector is 3.6 lp/mm, reconstructions of bar patterns have clearly shown higher frequencies due to super-resolution. In this paper, Figure 3(c) demonstrates that the ability to achieve super-resolution is influenced by focal spot motion, as the zeros of the modulation in a system with continuous tube motion vary with exposure time. A formula for these zeros is derived in the Appendix. Using high contrast bar patterns,[5] Figure 1 in our previous work demonstrated visibility of 6.0 lp/mm in the Selenia Dimensions system with a 3.7 s scan time and a 30.2 ms exposure time. For these settings, it follows from the Appendix that the modulation possesses a zero at 9.4 lp/mm. It is worth noting that if the same measurements were taken with the system's maximum exposure time of 50.0 ms, the limiting resolution of focal spot motion would be 5.6 lp/mm, and one would not expect the same 6.0 lp/mm bar patterns to be successfully resolved.

There has been recent interest in acquiring DBT images with less compression than conventional 2D mammography.[8] The purpose of the reduced compression is to spread out tissues and thus improve resolution in the z direction perpendicular to the breast support. This work argues against reduced compression, since it inherently leads to greater patient motion and would be expected to degrade the modulation of the reconstruction. In systems with long scan times, the need for full compression is particularly evident because the net object displacement should increase with scan time.

Some of the limitations of this study and directions for future modeling are now noted. Future work should more carefully model the MTF degradation due to non-normal x-ray incidence[9] as well as the finite size of the focal spot. In addition, the presence of noise at various radiation dose levels could be simulated. Although this work implicitly assumes a high contrast input frequency whose visibility is independent of dose, future studies should demonstrate how the optimization of scan time is influenced by noise at various dose levels for low contrast input frequencies. Because the attenuation coefficient of the input object is energy dependent, polyenergetic x-ray spectra should also be simulated. Furthermore, motion in the chest wall-to-nipple direction (y) should be simulated in addition to the x and z directions (Figure 2). Finally, while this work considers a constant object velocity, there are instances in which the velocity is expected to be time-dependent. For example, the velocity may be sinusoidal with time in order to simulate the pulsatile motion of structures lying along blood vessels.

5. ACKNOWLEDGEMENT

The authors thank Baorui Ren (Hologic Inc., Bedford, MA) for useful information on the acquisition geometry of the Selenia Dimensions DBT system. We are also grateful to Susan Ng (Real Time Tomography, LLC, Villanova, PA) for assistance in generating Figure 1. Andrew D. A. Maidment is the chair of the Scientific Advisory Board of Real Time Tomography. The project described was supported by predoctoral training Grant No. W81XWH-11-1-0100 through the Department of Defense Breast Cancer Research Program. The content is solely the responsibility of the authors and does not necessarily represent the official views of the funding agency.

6. APPENDIX

The MTF of the focal spot in a system with continuous x-ray tube motion is now calculated by analyzing rays emanating from different focal spot positions during a single projection. For the n^{th} projection, rays are first drawn between the point $(0, z_0)$ and the two endpoints of the tube arc. Subsequently, following Eq. (19), rays are backprojected toward the

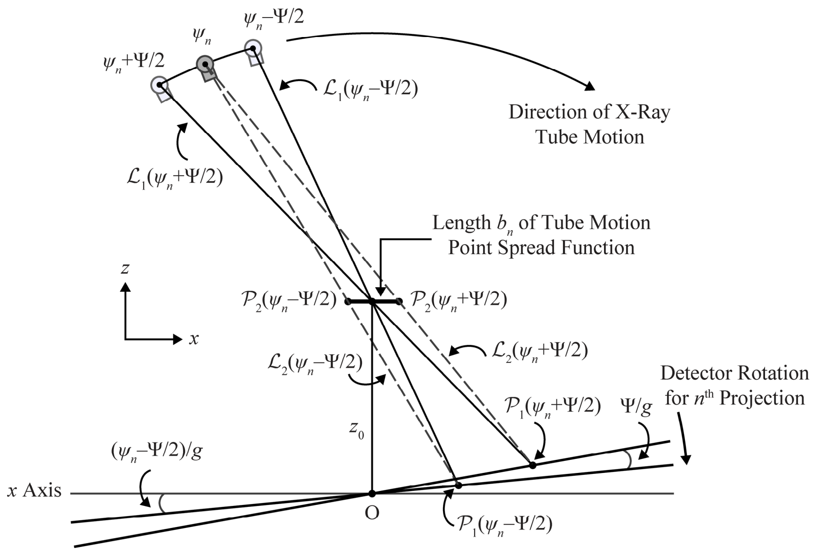

Figure 5. The point spread function (PSF) of focal spot motion is found by ray tracing.

nominal projection angle $\psi = \psi_n$. The length b_n between backprojected rays at the height $z = z_0$ yields a rectangle function corresponding to the PSF of tube motion. The MTF of focal spot motion is then calculated from the Fourier transform of the PSF. To implement this approach, it is first necessary to derive equations for the lines $\mathcal{L}_1(\psi_n + \Psi/2)$ and $\mathcal{L}_1(\psi_n - \Psi/2)$ between the point $(0, z_0)$ and the endpoints of the x-ray tube arc at $\psi = \psi_n + \Psi/2$ and $\psi = \psi_n - \Psi/2$. Since the focal spot coordinates are given by $x = -h\sin(\psi_n \pm \Psi/2)$ and $z = h\cos(\psi_n \pm \Psi/2)$, the rays through the point $(0, z_0)$ lie along the lines

$$\mathcal{L}_1(\psi_n \pm \Psi/2) = \left\{(x,z) : z = -\left[\cot(\psi_n \pm \Psi/2) - (z_0/h)\csc(\psi_n \pm \Psi/2)\right]x + z_0\right\}. \tag{A1}$$

The lines $\mathcal{L}_1(\psi_n + \Psi/2)$ and $\mathcal{L}_1(\psi_n - \Psi/2)$ strike the detector at the points $\mathcal{P}_1(\psi_n + \Psi/2)$ and $\mathcal{P}_1(\psi_n - \Psi/2)$, respectively

$$\mathcal{P}_1(\psi_n \pm \Psi/2) = \mathcal{L}_\mathcal{D}(\psi_n \pm \Psi/2) \cap \mathcal{L}_1(\psi_n \pm \Psi/2), \quad \mathcal{L}_\mathcal{D}(\psi_n \pm \Psi/2) = \left\{(x,z) : z = x\tan\left[(\psi_n \pm \Psi/2)/g\right]\right\} \tag{A2}$$

where $\mathcal{L}_\mathcal{D}(\psi_n + \Psi/2)$ and $\mathcal{L}_\mathcal{D}(\psi_n - \Psi/2)$ are lines along the length of the detector at the x-ray tube angles $\psi = \psi_n + \Psi/2$ and $\psi = \psi_n - \Psi/2$. Combining Eq. (A1) and (A2) gives

$$\mathcal{P}_1(\psi_n \pm \Psi/2) = (x,z) : x = z_0\chi_n^\pm \tan(\psi_n \pm \Psi/2),\ z = z_0\chi_n^\pm \tan\left[(\psi_n \pm \Psi/2)/g\right]\tan(\psi_n \pm \Psi/2), \tag{A3}$$

where

$$\chi_n^\pm = \left[1 + \tan\left[(\psi_n \pm \Psi/2)/g\right]\tan(\psi_n \pm \Psi/2) - (z_0/h)\sec(\psi_n \pm \Psi/2)\right]^{-1}. \tag{A4}$$

Signal at the detector positions $\mathcal{P}_1(\psi_n + \Psi/2)$ and $\mathcal{P}_1(\psi_n - \Psi/2)$ is in turn backprojected to the focal spot at the x-ray tube angle $\psi = \psi_n$, forming the lines $\mathcal{L}_2(\psi_n + \Psi/2)$ and $\mathcal{L}_2(\psi_n - \Psi/2)$.

$$\mathcal{L}_2(\psi_n \pm \Psi/2) = \left\{(x,z) : z = \frac{-\left[h\cos\psi_n - z_0\chi_n^\pm \tan\left[(\psi_n \pm \Psi/2)/g\right]\tan(\psi_n \pm \Psi/2)\right]\left[x + h\sin\psi_n\right]}{h\sin\psi_n + z_0\chi_n^\pm \tan(\psi_n \pm \Psi/2)} + h\cos\psi_n\right\} \tag{A5}$$

At the reconstruction depth $z = z_0$, the lines $\mathcal{L}_2(\psi_n + \Psi/2)$ and $\mathcal{L}_2(\psi_n - \Psi/2)$ intercept the two points $\mathcal{P}_2(\psi_n + \Psi/2)$ and $\mathcal{P}_2(\psi_n - \Psi/2)$.

$$\mathcal{P}_2(\psi_n \pm \Psi/2) = \mathcal{L}_2(\psi_n \pm \Psi/2) \cap \{(x,z) : z = z_0\} \tag{A6}$$

$$= (x,z) : x = \frac{\left[h \sin\psi_n + z_0 \chi_n^{\pm} \tan(\psi_n \pm \Psi/2)\right]\left[h\cos\psi_n - z_0\right]}{h\cos\psi_n - z_0\chi_n^{\pm}\tan\left[(\psi_n \pm \Psi/2)/g\right]\tan(\psi_n \pm \Psi/2)} - h\sin\psi_n,\ z = z_0 \tag{A7}$$

A rectangle function of length b_n is created between $\mathcal{P}_2(\psi_n + \Psi/2)$ and $\mathcal{P}_2(\psi_n - \Psi/2)$, thereby forming the effective PSF of the focal spot at the reconstruction depth $z = z_0$ (Figure 5). Using MATLAB, one can show that b_n does not vary significantly with projection number n for the Selenia Dimensions system. Consequently, the special case $n = 0$ is a useful approximation for the effective width of the PSF of focal spot motion in all projections.

$$b_0 = \frac{2z_0\left(1-\frac{z_0}{h}\right)\tan\left(\frac{\Psi}{2}\right)}{1+\tan\left(\frac{\Psi}{2g}\right)\tan\left(\frac{\Psi}{2}\right) - \frac{z_0}{h}\left[\sec\left(\frac{\Psi}{2}\right)+\tan\left(\frac{\Psi}{2g}\right)\tan\left(\frac{\Psi}{2}\right)\right]} \cong \frac{2z_0\left(1-\frac{z_0}{h}\right)\tan\left(\frac{\Psi}{2}\right)}{1-\frac{z_0}{h}\sec\left(\frac{\Psi}{2}\right)} = \frac{2z_0\left(1-\frac{z_0}{h}\right)\tan\left[\left(\frac{N-1}{T_t-\tau}\right)\frac{\tau\Delta\psi}{2}\right]}{1-\frac{z_0}{h}\sec\left[\left(\frac{N-1}{T_t-\tau}\right)\frac{\tau\Delta\psi}{2}\right]} \tag{A8}$$

Since $\Psi/2$ is well under 1° for typical acquisition geometries, one can use the approximation $\tan[\Psi/(2g)]\tan(\Psi/2) \ll 1$ to derive this result. With the PSF of focal spot motion given by $\text{rect}(x/b_0)$, the MTF of focal spot motion is thus $\text{sinc}(b_0 f)$. The zeros of this MTF are integer multiples of $1/b_0$. This formula perfectly calculates the zeros of the modulation of the reconstruction in Figure 3(c) for a system with continuous tube motion and no patient motion.

7. REFERENCES

1. Rafferty EA. Tomosynthesis: New Weapon in Breast Cancer Fight. *Decisions in Imaging Economics.* April 2004 2004;17(4).

2. Ren B, Ruth C, Stein J, Smith A, Shaw I, Jing Z. Design and performance of the prototype full field breast tomosynthesis system with selenium based flat panel detector. Paper presented at: SPIE, 2005; San Diego, CA.

3. Zhao B, Zhao W. Three-dimensional linear system analysis for breast tomosynthesis. *Medical Physics.* 2008;35(12):5219-5232.

4. Bissonnette M, Hansroul M, Masson E, et al. Digital breast tomosynthesis using an amorphous selenium flat panel detector. Paper presented at: SPIE, 2005; San Diego, CA.

5. Acciavatti RJ, Maidment ADA. Investigating the Potential for Super-Resolution in Digital Breast Tomosynthesis. Paper presented at: SPIE, 2011; Lake Buena Vista, FL.

6. Lee DL, Cheung LK, Rodricks B, Powell GF. Improved imaging performance of a 14 x 17-inch Direct Radiography (TM) System using Se/TFT detector. Paper presented at: SPIE Conference on Physics of Medical Imaging, 1998; San Diego, CA.

7. Acciavatti RJ, Maidment ADA. A Comparative Analysis of OTF, NPS, and DQE in Energy Integrating and Photon Counting Digital X-ray Detectors. *Medical Physics.* 2010;37(12):6480-6495.

8. Fornvik D, Andersson I, Svahn T, Timberg P, Zackrisson S, Tingberg A. The Effect of Reduced Breast Compression in Breast Tomosynthesis: Human Observer Study Using Clinical Cases. *Radiation Protection Dosimetry.* 2010;139(1-3):118-123.

9. Hajdok G, Cunningham IA. Penalty on the detective quantum efficiency from off-axis incident x rays. Paper presented at: Medical Imaging 2004: Physics of Medical Imaging, 2004; San Diego, CA.